ACS Catalysis

Research Article

pubs.acs.org/acscatalysis

Aligned Nanoporous Pt−Cu Bimetallic Microwires with High Catalytic Activity toward Methanol Electrooxidation

H.-J. Qiu,[†,‡] X. Shen,[†] J. Q. Wang,[†] A. Hirata,[†] T. Fujita,[†] Y. Wang,[*,‡] and M. W. Chen[*,†,§]

[†]WPI Advanced Institute for Materials Research, Tohoku University, Sendai 980-8577, Japan

[‡]School of Chemistry and Chemical Engineering, Chongqing University, Chongqing 400044, China

[§]State Key Laboratory of Metal Matrix Composites, School of Materials Science and Engineering, Shanghai Jiao Tong University, Shanghai 200030, China

Supporting Information

ABSTRACT: We report a simple approach to fabricate aligned bimetallic Pt−Cu microwires with a three-dimensional nanoporous structure, tunable composition, and high catalytic activity by dealloying a dilute Pt_3Cu_{97} precursor. Each microwire possesses inherent ultrafine nanoporous structure with uniformly distributed Pt−Cu alloy ligaments and nanopores with a dimension of ∼2 nm. Electrochemical measurements manifest that the nanoporous Pt−Cu microwires have significantly enhanced electrocatalytic activities compared with a commercial Pt/C nanoparticulate catalyst. With evident advantages of facile preparation and enhanced catalytic performance together with low material costs, the nanoporous Pt−Cu microwires hold great promise as a high-performance catalyst for electrochemical energy conversion.

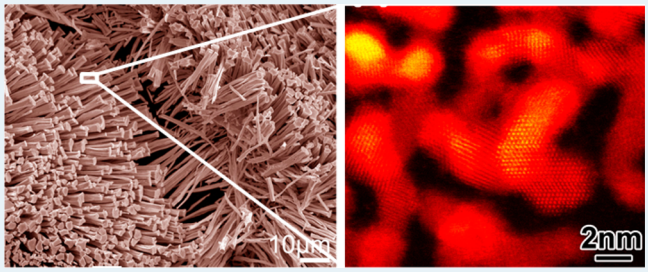

KEYWORDS: *nanoporous metals, core/shell structure, dealloying, methanol oxidation, electrocatalysts, bimetallic Pt catalysts, fuel cells*

INTRODUCTION

Platinum-based catalysts have been widely investigated because of their important applications in energy conversion and storage.[1−9] The high material costs and low natural reservation of Pt have stimulated extensive studies to search low-Pt or even Pt-free catalysts with retained high catalytic properties. It has recently been found that bimetallic Pt alloys containing low-cost transition metals (such as Cu, Ni, Fe, Pb, etc.) can effectively reduce the loading amount of Pt and have enhanced catalytic activities in comparison with pure Pt counterparts.[7−19] The enhanced catalytic performances originate from the electronic structure optimization that is associated with the formation of a core−shell structure consisting of a Pt-rich shell and a low-Pt alloy core, as well as nanoscale surface strains. Moreover, it is known that Pt catalysts are often poisoned by carbonaceous intermediates generated during organic molecule oxidation. The transition metal components in the low-Pt bimetallic catalysts can effectively improve the poisoning tolerance of Pt catalysts by removing carbonaceous molecules during oxidation reactions.

To fabricate bimetallic Pt-based nanoparticulate catalysts, many strategies have been proposed, such as hydrothermal reduction, electrodeposition, etc.;[20−25] however, it is difficult to manage the composition and geometry of the Pt-based bimetallic catalysts simultaneously by these bottom-up approaches. More recently, dealloying has been proved to be an effective way to fabricate nanostructured bimetallic catalysts with a bicontinuous open nanoporous structure and large effective surface area.[26−31] Different from the bottom-up approaches, the dealloying method can well control the compositions of bimetallic catalysts by etching away an excess component from a predetermined ternary alloy[32,33] or by tuning the dealloying potentials of a binary alloy. Because there are only a few single-phase ternary Pt-based alloys available in the equilibrium phase diagrams, it is more practical to fabricate bimetallic Pt-based catalysts by dealloying binary Pt alloys in a controllable manner. In our previous studies, we have successfully fabricated bimetallic nanoporous Pt−Cu (np-PtCu) and Pd−Ni catalysts with tunable Pt/Cu and Pd/Ni ratios by controlling the dealloying potentials of $Pt_{15}Cu_{85}$ and $Pd_{20}Ni_{80}$ precursor alloys, respectively.[26,31]

To further decrease the loading amount of noble metals and enlarge the tunable composition range of the nanoporous bimetallic catalysts, reducing the concentrations of noble metal components in precursor alloys is preferred. However, the dealloying approach usually requires that the concentration of a noble-metal component fall in the range of 15−45 at. % in binary precursors.[34] Larger than 45 at. % usually results in surface passivation that prevents the formation of a nanoporous structure, and lower than 15 at. % leads to fragmentation of the resultant porous materials. By modifying the microstructure of a precursor alloy and optimizing the dealloying conditions, in

Received: January 15, 2015
Revised: April 9, 2015
Published: May 12, 2015

DOI: 10.1021/acscatal.5b00073
ACS Catal. 2015, 5, 3779−3785

this study we have successfully fabricated aligned nanoporous Pt−Cu (np-PtCu) microwires using a diluted Pt_3Cu_{97} precursor. The novel np-PtCu microwires with a tunable Pt/Cu ratio, lower Pt loading amount, and ultralarge effective surface area show superior electrocatalytic activities toward methanol electrooxidation in comparison with commercial Pt/C nanoparticulate catalysts.

EXPERIMENTAL METHODS

Material Fabrication. Pt_3Cu_{97} alloy ribbons with a thickness of ∼25−30 μm were prepared using an induction melt spinning method. The sample chamber was first pumped to high vacuum (<0.003 Pa) and then backfilled with high-purity Ar gas for protection. The pure Pt and Cu (>99.9%) were melted in a quartz tube, followed by injection onto a rotating Cu wheel (tangent speed, 20 m s^{-1}) to obtain the alloy ribbons. The cold Cu wheel produced a large temperature gradient across the thickness of the Pt_3Cu_{97} ribbons, leading to the formation of a columnar grain structure that is vertical to the ribbon surfaces. Nanoporous PtCu microwires were prepared by chemically dealloying the binary alloy in a diluted HNO_3 solution at room temperature. The catalyst suspensions were made by ultrasonicating a mixture of 3.0 mg of nanoporous PtCu microwires, 4.0 mg of carbon powder, 300 μL of isopropyl alcohol, and 100 μL of a Nafion solution (0.5 wt %) for 20 min. Four microliters of the catalyst suspension was dropped onto a glassy carbon electrode as the working electrode. The Johnson-Matthey Pt/C catalyst (20 wt % on carbon powder, Alfa Aesar) was used as the reference.

Microstructure Characterization. The crystal structures were investigated by X-ray diffraction (XRD) on a Bruker D8 Advance X-ray diffractometer using Cu Kα radiation. The microstructures were characterized on a JEM-2100 high-resolution transmission electron microscope (HRTEM) and a JSM-6700 field-emission scanning electron microscope (SEM) equipped with an energy-dispersive X-ray spectrometer (EDS). The surface chemical state was analyzed by X-ray photoelectron spectroscopy (XPS, AxIS-ULTRA-DLD) with an Al Kα (mono) anode at the energy of 150 W in a vacuum of 10^{-7} Pa.

Evaluation of Electrocatalytic Activity. Electrochemical tests were performed on an electrochemical workstation (Iviumstat Technology) at room temperature. A three-electrode cell was used with the catalyst-modified glassy carbon electrode (3 mm in diameter) as the working electrode, a Pt foil as the counter electrode, and a saturated calomel electrode (SCE) as the reference electrode. All potentials were referred to SCE. To facilitate the electrochemical test, we mix the np-PtCu wires, Nafion, and carbon power by ultrasonication to prepare the catalyst suspension that is coated on glassy carbon electrode for the test. The addition of carbon powder would help the formation of the suspension to form a uniformly thin coating on the glassy carbon electrode. Electrolyte solutions were deoxygenated by bubbling with high-purity N_2 for ∼20 min prior to measurements. The electrochemically active surface area (EASA) of Pt was measured by integrating the charges associated with hydrogen adsorption between −0.2 and 0.1 V and calibrated by the adsorption (210 μC cm^{-2}_{Pt}) of a monolayer of hydrogen on a polycrystalline Pt surface.[2]

RESULTS AND DISCUSSION

The Pt_3Cu_{97} alloy ribbons were examined by XRD (Figure 1a) and EDS (Figure S1a in the Supporting Information). Only

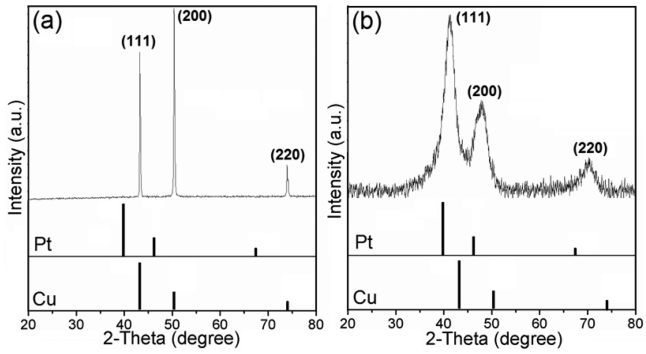

Figure 1. XRD patterns of the Pt_3Cu_{97} alloy before (a) and after (b) 24 h of dealloying in a 8 M HNO_3 solution. The standard patterns of Pt (JCPDS 65-2868) and Cu (JCPDS 04-0836) are included for comparison.

three diffraction peaks appear in the XRD spectra, which can be assigned as (111), (200), and (220) diffractions of a face-centered-cubic (fcc) phase. Because the content of Pt is very low (∼3 at. %) in the alloy, the positions of three diffraction peaks are very close to those of pure Cu. It is worth noting that the as-prepared ribbons show a much stronger peak intensity of (200), in comparison with the standard FCC diffraction patterns, suggesting the formation of (200) texture (most columnar grains align along the [200] direction) in the rapidly quenched ribbons. After 24 h of dealloying in 8 M HNO_3 solution, the color of the Pt_3Cu_{97} precursor turns to black from its original brown, indicating the selective leaching of Cu from the alloy. The XRD pattern of the dealloyed sample (Figure 1b) shows that the original diffraction peaks of the Pt_3Cu_{97} alloy completely disappeared and, instead, three new diffraction peaks located at 41.2, 47.7, and 70.7° (2θ) appeared, which can be ascribed to the (111), (200), and (220) diffractions of a fcc structure. These peaks are located between the diffraction peaks of pure Pt and Cu, indicating the alloy nature of the reaction product. EDS measurements of the dealloyed sample (Figure S1b) suggest that the atomic ratio of Pt and Cu is ∼60:40, which is in good agreement with the calculations based on the XRD result and Vegrad's law. The broad diffraction peaks of the dealloyed sample imply the formation of a nanoscale structure.

From the plane-view SEM image of the dealloyed sample (Figure 2a), one can clearly observe that the solid and continuous ribbon cracks into ∼1−3 μm discrete domains separated by microscale void channels. The section-view SEM image (Figure 2b) shows that these solid domains are actually the cross sections of aligned microwires with a uniform length of ∼30 μm. These aligned microwires are weakly interconnected and can be handled as a free-standing film; however, a mild ultrasonication treatment can separate the microwires as suspending individual microwires in solutions (Figure 2c and Figure S2). The transmission electron microscopy (TEM) image (Figure 2d) shows that the microwires are porous with metallic ligament and nanopore sizes of ∼2 nm. The polycrystalline rings in the selected area electron diffraction (SAED) pattern (inset in Figure 2d) and the continuous lattice fringes from a HRTEM image (Figure S3) indicate the crystalline nature of the ligaments. The high-angle annular dark-field scanning TEM (HAADF-STEM) images (Figure 2e,f) further demonstrate the ligament−pore structure with an obvious contrast difference between the bright metallic ligaments and the dark pores. From the zoom-in STEM

DOI: 10.1021/acscatal.5b00073
ACS Catal. 2015, 5, 3779−3785

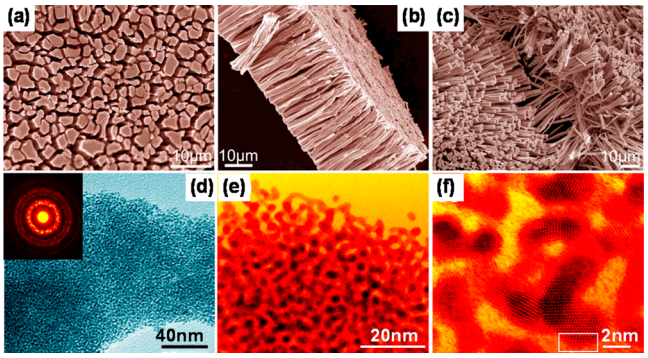

Figure 2. SEM images of the dealloyed sample: plane-view image (a), section-view image (b), image of a mildly crushed one (c). TEM (d) and high-angle annular bright field STEM (e, low magnification; f, high magnification) images of the np-PtCu microwires. Inset in part d is the corresponding SAED image.

image (Figure 2f), the atomic structure of the ultrafine Pt−Cu ligament can be clearly observed. The ligament surface exhibits a large number of surface steps and kinks. These defect sites (one part is denoted by a white rectangle) are expected to correspond to the high catalytic activities of the np-PtCu microwires.[35]

The composition and valence state of the np-$Pt_{60}Cu_{40}$ microwires were further examined by X-ray photoelectron spectroscopy (XPS). Two Pt 4f peaks were located at 71.5 and 74.8 eV (Figure 3a), which can be assigned to the Pt $4f_{7/2}$ and

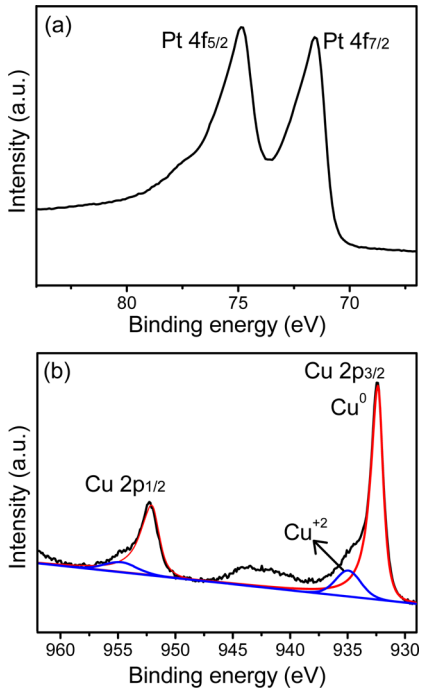

Figure 3. XPS spectra of the Pt 4f (a) and Cu 2p (b) of np-$Pt_{60}Cu_{40}$ microwires.

Pt $4f_{5/2}$ of metallic Pt^0, respectively. Compared with that of pure Pt (71.2 eV), the Pt $4f_{7/2}$ binding energy of the np-PtCu shifts positively, indicating the changes in the electronic structure, probably due to the charge transfer between Cu and Pt. The positive shift suggests a lower density of valence electrons (5d) of the Pt−Cu alloy than that of pure Pt.[36] The Cu 2p spectrum (Figure 3b) shows that, although most of the Cu is in the form of metallic Cu^0 (932.4 eV), a weak signal from Cu^{II} (935.0 eV) also exists. The presence of a small amount of Cu^{II}, further confirmed by a satellite peak at ∼943 eV, can be attributed to the oxidation of surface Cu atoms in air. On the basis of the XPS analysis, the average composition from the top surface region is about $Pt_{77}Cu_{23}$. The higher Pt content in the surface region than the overall $Pt_{60}Cu_{40}$ indicates the ligaments of the nanoporous PtCu have a Pt-rich outmost surface. Moreover, after 1 min of gentle Ar ion etchin,g which partly removes the outmost surface, the XPS result shows that the new surface has a composition of ∼$Pt_{74}Cu_{26}$. The increased Cu content in the sublayer further demonstrates the Pt-rich surface of the dealloyed nanoporous PtCu. Although the XPS data cannot provide direct evidence on the formation of a core−shell structure, the composition variation indicates that the ligament surface contains a relatively high Pt amount. This result is also consistent with the wide range of observations of a noble metal-rich surface in dealloyed bimetallic catalysts.[17,18,26,31,33]

For single-phase binary precursors with a suitable composition (noble component: ∼15−45 at. %), the original grain morphology and crystal orientation can be well preserved in the resulting nanoporous products after dealloying. Meanwhile, obvious volume shrinkage together with large internal strains can be produced by dealloying.[37] In this work, the formation of an aligned microwire-like structure is apparently associated with the anisotropic volume shrinking of individual columnar grains in the precursor alloys. Because the length of the nanoporous microwires is close to the original thickness of the precursor ribbons, the lateral shrinkage perpendicular to the ⟨100⟩ orientation appears more significant, leading to the separation of individual columnar grains to form the aligned nanoporous microwires.

To demonstrate this, a time-dependent dealloying experiment was carried out (Figure 4). Before dealloying, voids cannot be seen in the polycrystalline precursor (Figure 4a). After 5 min of dealloying, the columnar grains begin to be separated from each other, and voids form at grain boundaries (GBs) (Figure 4b). In addition to the anisotropic volume shrinkage, the preferred formation of voids at GBs may also be related to possible GB segregations of less-noble Cu. After 30 min of dealloying, large voids between columnar grains can be observed, resulting in well-aligned nanoporous microwires (Figure 4c). The selective dissolution of the solvent Cu from the dilute Pt_3Cu_{97} solid solution naturally produces a more porous space, significant lattice distortion, and large volume shrinkage, promoting the formation of the separate nanoporous microwires. To verify the effect of the Cu content on the formation of nanoporous microwires, we investigated the dealloying process of a $Pt_{15}Cu_{85}$ alloy. As shown in Figure S4a, after 24 h of dealloying of the $Pt_{15}Cu_{85}$ precursor in 8 M HNO_3 solution, the grain separation can occasionally be seen, and most GBs remain the same as the original alloy precursor. This indicates that the extremely low concentration of Pt is critical for the formation of separate nanoporous microwires. EDS analysis (Figure S4b) shows that the residual Cu concentration in the dealloyed $Pt_{15}Cu_{85}$ alloy is only ∼5 at. %, which is much lower than that (40 at. %) in the dealloyed Pt_3Cu_{97} precursor under the same dealloying conditions (24 h, 8 M HNO_3 solution). We noticed that the PtCu ligament size (∼2 nm) in the nanoporous microwires is much smaller than that (>5 nm) in the dealloyed $Pt_{15}Cu_{85}$. This indicates that the obvious

DOI: 10.1021/acscatal.5b00073
ACS Catal. 2015, 5, 3779−3785

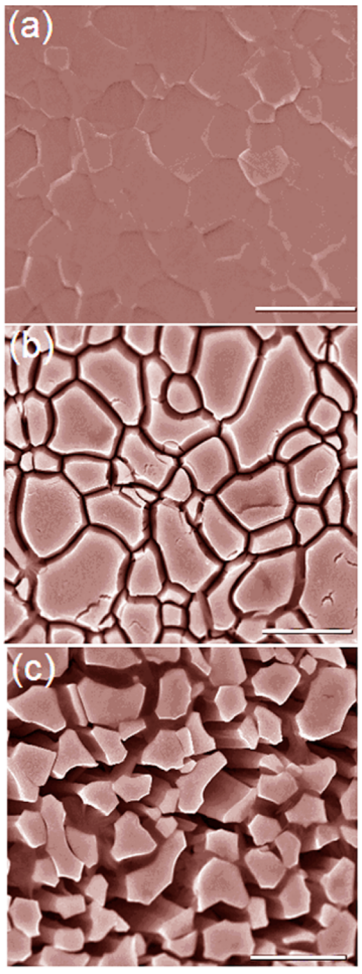

Figure 4. SEM images of the Pt_3Cu_{97} alloy after dealloying for 0 (a), 2 (b), and 30 min (c) in a 8 M HNO_3 solution. Scale bar: 5 μm.

difference in the contents of residual Cu could be associated with the critical size for selective etching at which the surface potentials play a more important role than that of chemical potential difference between the constituent elements and, hence, prevent the further development of selective etching.

To tune the composition of the np-PtCu microwires, we systematically studied the composition evolution with dealloying time in the 8 M HNO_3 solution. As shown in Figure 5a, the Cu content quickly decreases to ~44 at. % in the first 30 min and then changes slowly. A nanoporous $Pt_{60}Cu_{40}$ can be obtained after 24 h of dealloying. On the other hand, no obvious microstructure coarsening can be observed, even after dealloying for 72 h, which is in contrast to nanoporous Au by dealloying a AuAg alloy.[38] This phenomenon could be associated with the much slower surface diffusivity of Pt (~3.6×10^{-22} cm^2 s^{-1} in vacuum) than that of Au (~2.2×10^{-19} cm^2 s^{-1} in vacuum).[39]

We also investigated the effect of acid solutions on the chemical composition and morphology of np-PtCu microwires. After 24 h of dealloying in HNO_3 solutions with three different concentrations of 1.6, 8.0, and 12.8 M HNO_3 (Figure 5b), the obtained np-PtCu microwires have a compositions of $Pt_{53}Cu_{47}$, $Pt_{60}Cu_{40}$ and $Pt_{70}Cu_{30}$, respectively. For comparison, SEM and EDS characterizations of the representative np-$Pt_{70}Cu_{30}$ are shown in Figure S5. The Cu contents of all three samples changes negligibly after extending the dealloying time longer than 24 h.

The np-PtCu microwires with tunable compositions were evaluated as a potential anodic catalyst in direct methanol fuel cells. Figure S6 shows cyclic voltammetry (CV) curves of three representative np-PtCu catalysts in a 0.5 M H_2SO_4 solution. For comparison, the CV curve of the commercial Pt/C catalyst is also included in the plot. All of the Pt−Cu catalysts show characteristic CV curves of Pt. The peaks in the region between −0.2 and 0.1 V can be attributed to the adsorption and desorption of hydrogen. Between 0.1 and 0.3 V is the double-layer region, and at higher potentials it is the region of surface oxidation and subsequent reduction of Pt during the backward scan. It is noticed that for the Pt−Cu catalysts, there is a small anodic peak at ~0.5 V during the forward scan, which can be attributed to the oxidation of residual surface Cu. The invariability of this peak during the first several CV scans indicates that the small amount of surface Cu atoms is stabilized by Pt. In comparison, the peak of Cu oxidation on $Pt_{53}Cu_{47}$ catalyst is located at a higher potential than those on $Pt_{70}Cu_{30}$ and $Pt_{60}Cu_{40}$. Moreover, compared with Pt/C, the reduction peaks of the surface oxides on all the np-PtCu catalysts shift to a higher potential (denoted by the dot line), indicating the weak interaction between Pt and oxygenated species. On the basis of the hydrogen adsorption charge, the EASA of the np-PtCu is determined to be ~53 m^2 g^{-1}, which is comparable with that of the commercial Pt/C (62 m^2 g^{-1}). The large EASA apparently results from the ultrafine nanoporous structure of the np-PtCu with ligament and pore sizes of ~2 nm and is much higher than other reported PtCu nanomaterials, such as Pt nanodendrites (23.5 m^2 g^{-1})[8] with an average crystal size of ~5 nm and PtCu nanocages (35.7 m^2 g^{-1}).[16]

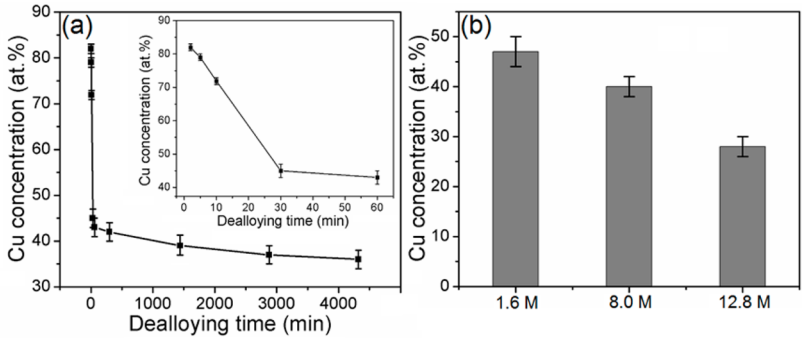

Figure 5. Residual Cu concentrations of np-PtCu microwires (measured by EDS) with different dealloying times in a 8 M HNO_3 solution (a) and after 24 h of dealloying with different HNO_3 concentrations (b). The inset in part a is the enlarged figure of part a from 0 to 60 min.

DOI: 10.1021/acscatal.5b00073
ACS Catal. 2015, 5, 3779−3785

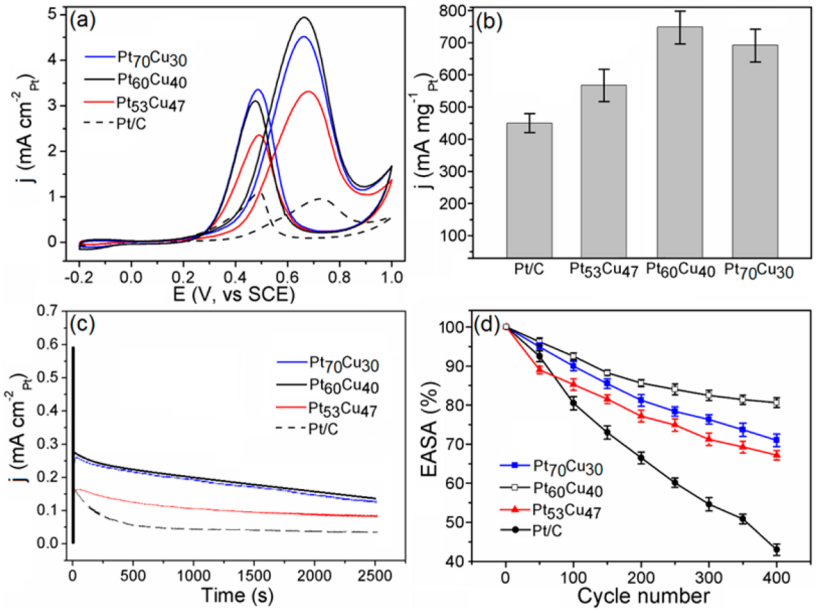

Figure 6. CV curves (a), Pt mass-specific peak current densities (b), and current−time curves (at 0.4 V, (c)) of nanoporous $Pt_{53}Cu_{47}$, $Pt_{60}Cu_{40}$, $Pt_{70}Cu_{30}$, and Pt/C catalysts in 0.5 M H_2SO_4 + 1.0 M CH_3OH solution. Loss of EASAs of the four catalysts with increasing scan cycles (from −0.2 to 1.0 V, (d)). Scan rate: 50 mV s^{-1}.

Figure 6a shows the CV curves of the np-PtCu and Pt/C catalysts in a 0.5 M H_2SO_4 + 1 M CH_3OH aqueous solution. The current densities have been normalized by the EASA of Pt. For all the catalysts, the peak between 0.6 and 0.7 V in the forward scan is attributed to the electrooxidation of methanol. The anodic peak at ∼0.5 V in the backward scan is associated with the reactivation of oxidized Pt.[40] For the np-PtCu microwires, the peak potentials in the forward scan is located at ∼0.65 V, obviously lower than that of Pt/C (0.72 V), indicating the facilitated reaction kinetics for methanol dehydrogenation on the np-PtCu electrodes. More importantly, the specific peak current densities on the np-PtCu catalysts are ∼4.9 ($Pt_{60}Cu_{40}$), ∼4.5 ($Pt_{70}Cu_{30}$), and ∼3.3 ($Pt_{53}Cu_{47}$) mA cm^{-2}, which are much higher than that on the Pt/C catalyst (∼1.0 mA cm^{-2}). Noticeably, the peak current density of np-$Pt_{60}Cu_{40}$ is ∼5 times larger than that of Pt/C catalyst, which is also much higher than those on dendritic Pt−Cu nanocrystals (∼0.96 mA cm^{-2})[41] and comparable to that on Pt−Cu nanocubes (∼4.7 mA cm^{-2}).[42] These results further confirm the high catalytic activity of the np-PtCu microwires. As shown in Figure 6b, the np-$Pt_{60}Cu_{40}$ catalyst also exhibits the highest mass specific activity (∼750 mA mg^{-1}_{Pt}) among the four catalysts in this study, which is also one of the highest values of the Pt-based catalysts reported in the literature.[2,11,16,23]

The peak current density ratio of the forward (I_f) and backward scans (I_b) has been used to evaluate the poisoning tolerance of a catalyst. A higher I_f/I_b value indicates a better poisoning tolerance. As calculated from Figure 6a, the I_f/I_b of Pt/C catalyst is 0.88, which is in fair agreement with those reported elsewhere.[41] The I_f/I_b ratios for np-$Pt_{60}Cu_{40}$, $Pt_{70}Cu_{30}$, and $Pt_{53}Cu_{47}$ are 1.58, 1.34, and 1.43, respectively. Compared with that of Pt/C, the higher values from the Pt−Cu catalysts suggest the better tolerance to poisoning. The enhanced tolerance to poisoning may be related to the weak adsorption of CO on the Pt−Cu catalyst surface,[43] which is somewhat in line with the observation that the smallest I_f/I_b ratio is from $Pt_{70}Cu_{30}$ with a more Pt-rich surface.

Figure 6c presents current−time curves of these catalysts in a 0.5 M H_2SO_4 + 1.0 M CH_3OH solution at 0.4 V. The steady-state currents on the np-PtCu electrodes are much higher than that on the commercial Pt/C catalyst, which is consistent with the CV measurements and further demonstrates the enhanced catalytic activity of the np-PtCu microwires. Moreover, after 2500 s running, the current densities retain ∼65% of their initial values for $Pt_{60}Cu_{40}$ and $Pt_{70}Cu_{30}$, ∼51% for $Pt_{53}Cu_{47}$, and only ∼24% for Pt/C, indicating that a suitable amount of Cu can effectively reduce the activity decay of Pt-based catalysts.

The stability of the electrocatalysts was also evaluated by continuous CV cycling from −0.2 to 1.0 V in a 0.5 M H_2SO_4 solution. As shown in Figure 6d, the EASAs of all the catalysts decrease with increasing scan cycles. The np-PtCu catalysts retain ∼80% ($Pt_{60}Cu_{40}$), ∼71% ($Pt_{70}Cu_{30}$), and ∼67% ($Pt_{53}Cu_{47}$) of their initial values after 400 cycles, whereas the EASA of the commercial Pt/C catalyst drops to ∼43% of its initial value under the same testing conditions. Similar to the Pt nanoparticles, the degradation of the np-PtCu catalyst is mainly due to the loss of EASA by nanostructure coarsening. As shown in Figure S7, the ligament size increases to ∼4−6 nm after 400 CV cycles. For the nanoparticulate Pt catalyst, the loss of EASA is caused by nanoparticle aggregatio and the detachment from the conductive carbon supports;. however, for the nanoporous catalyst, the EASA loss results from the ligament surface reconstruction and ligament coarsening.[32] Additionally, XPS analysis shows that the continuous CV cycling also causes further dissolution of Cu from the ligament surface. After 400 cycles, Cu can be barely detected from the surface region. Therefore, it is expected that the stability of the np-PtCu catalyst can be further improved by preventing the coarsening of nanoporous structure and continuous dissolution of the less-noble element.

For the origin of the greatly enhanced catalytic performance of the np-PtCu microwires, the following aspects should be mentioned. First, the bicontinuous nanoporous structure in the microwires provides excellent electron conductivity for Pt

DOI: 10.1021/acscatal.5b00073
ACS Catal. 2015, 5, 3779−3785

surface sites, which can effectively utilize the catalytically active surfaces for enhanced reaction kinetics. Second, the nanoscale core/shell structure with Pt-rich shell and Pt−Cu alloy core may allow greatly enhanced catalytic reactivity as a result of possible electronic, strain, and alloy effects.[44−47] It has been suggested that alloying Pt with other metals can lower the electronic binding energy in Pt and promote the C−H cleavage reaction at a lower potential. Third, the large open space between individual nanoporous microwires facilitates mass transport during the electrode reactions, in comparison with the bulk nanoporous Pt−Cu catalysts,[31] which definitely promote the electrode reaction kinetics. Finally, a one-dimensional structure (such as nanowires and nanorods) has been reported to possess an enhanced catalytic activity due to its uniquely anisotropic nature, which imparts advantageous structural and electronic factors in the catalytic reactions.[48,49]

On the basis of these arguments, it is not surprising that the present np-PtCu microwires exhibit significantly enhanced catalytic activities toward methanol electrooxidation. For the three np-PtCu microwire catalysts, $Pt_{60}Cu_{40}$ and $Pt_{70}Cu_{30}$ show a better catalytic performance than $Pt_{53}Cu_{47}$, which may result from the more Pt-rich surface because the electrooxidation of methanol involves multistep adsorption and electron transfer and requires various adjacent Pt active sites.[40] On the other hand, relatively less Cu in the Pt−Cu alloy core may give rise to an optimally strained Pt out-layer in the core/shell nanostructure.[50,51]

CONCLUSIONS

Aligned np-PtCu microwire catalysts with inherent nanoporous structure and tunable composition have been fabricated by one-step dealloying of a dilute Pt_3Cu_{97} precursor. The obtained nanoporous bimetallic catalysts have a core/shell structure with a noble metal-rich surface and a Pt−Cu alloy core. Importantly, the hierarchical np-PtCu catalysts show dramatically enhanced catalytic activities toward methanol oxidation for direct methanol fuel cells. The present fabrication strategy without the use of any organic solvent or surfactant provides a simple and controllable approach for fabricating massive nanoporous bimetallic microwires with high catalytic activity for applications in electrochemical energy conversion and storage.

ASSOCIATED CONTENT

Supporting Information

The Supporting Information is available free of charge on the ACS Publications website at DOI: 10.1021/acscatal.5b00073.

EDS, SEM, TEM, and electrochemical data (PDF)

AUTHOR INFORMATION

Corresponding Authors

*E-mail: wangy@cqu.edu.cn.

*E-mail: mwchen@wpi-aimr.tohoku.ac.jp.

Notes

The authors declare no competing financial interest.

ACKNOWLEDGMENTS

This work was sponsored by JST-CREST "Interface Science for Highly Efficient Energy Utilization", JST; "World Premier International Research Center (WPI) Initiative" by MEXT, Japan; the Thousand Young Talents Program of the Chinese Central Government (No. 0220002102003); the National Natural Science Foundation of China (No. 21373280); and the Hundred Talents Program at Chongqing University (No. 0903005203205).

REFERENCES

(1) Snyder, J.; Fujita, T.; Chen, M. W.; Erlebacher, J. *Nat. Mater.* **2010**, *9*, 904−907.

(2) Liu, L. F.; Pippel, E.; Scholz, R.; Gosele, U. *Nano Lett.* **2009**, *9*, 4352−4358.

(3) Shui, J. I.; Chen, C.; Li, J. C. M. *Adv. Funct. Mater.* **2011**, *21*, 3357−3362.

(4) Lu, Y.; Jiang, Y.; Wu, H.; Chen, W. *J. Phys. Chem. C* **2013**, *117*, 2926−2938.

(5) Lu, Y.-C.; Xu, Z.; Gasteiger, H. A.; Chen, S.; Hamad-Schifferli, K.; Shao-Horn, Y. *J. Am. Chem. Soc.* **2010**, *132*, 12170−12171.

(6) Guo, S.; Dong, S.; Wang, E. *Chem. Commun.* **2010**, *46*, 1869−1871.

(7) Stamenkovic, V. R.; Mun, B. S.; Mayrhofer, K. J. J.; Ross, P. N.; Markovic, N. M. *J. Am. Chem. Soc.* **2006**, *128*, 8813−8819.

(8) Gong, M.; Fu, G.; Chen, Y.; Tang, Y.; Lu, T. *ACS Appl. Mater. Interfaces* **2014**, *6*, 7301−7308.

(9) Yamauchi, Y.; Tonegawa, A.; Komatsu, M.; Wang, H.; Wang, L.; Nemoto, Y.; Suzuki, N.; Kuroda, K. *J. Am. Chem. Soc.* **2012**, *134*, 5100−5109.

(10) Guo, S.; Sun, S. *J. Am. Chem. Soc.* **2012**, *134*, 2492−2495.

(11) Kang, Y.; Pyo, J. B.; Ye, X.; Gordon, T. R.; Murray, C. B. *ACS Nano* **2012**, *6*, 5642−5647.

(12) Park, K.-W.; Choi, J.-H.; Sung, Y.-E. *J. Phys. Chem. B* **2003**, *107*, 5851−5856.

(13) Wu, J.; Gross, A.; Yang, H. *Nano Lett.* **2011**, *11*, 798−802.

(14) Yin, A.-X.; Min, X.-Q.; Zhang, Y.-W.; Yan, C.-H. *J. Am. Chem. Soc.* **2011**, *133*, 3816−3819.

(15) Yu, Y.; Yang, W.; Sun, X.; Zhu, W.; Li, X. Z.; Sellmyer, D. J.; Sun, S. *Nano Lett.* **2014**, *14*, 2778−2782.

(16) Xia, B. Y.; Wu, H. B.; Wang, X.; Lou, X. W. *J. Am. Chem. Soc.* **2012**, *134*, 13934−13937.

(17) Strasser, P.; Koh, S.; Anniyev, T.; Greeley, J.; More, K.; Yu, C. F.; Liu, Z. C.; Kaya, S.; Nordlund, D.; Ogasawara, H.; Toney, M. F.; Nilsson, A. *Nat. Chem.* **2010**, *2*, 454−460.

(18) Koh, S.; Strasser, P. *J. Am. Chem. Soc.* **2007**, *129*, 12624−12625.

(19) Neyerlin, K. C.; Srivastava, R.; Yu, C.; Strasser, P. *J. Power Sources* **2009**, *186*, 261−267.

(20) Chen, A.; Holt-Hindle, P. *Chem. Rev.* **2010**, *110*, 3767−3804.

(21) Wang, D.; Li, Y. *Adv. Mater.* **2011**, *23*, 1044−1060.

(22) Choi, S.-I.; Xie, S.; Shao, M.; Odell, J. H.; Lu, N.; Peng, H.-C.; Protsailo, L.; Guerrero, S.; Park, J.; Xia, X.; Wang, J.; Kim, M. J.; Xia, Y. *Nano Lett.* **2013**, *13*, 3420−3425.

(23) Wang, L.; Yamauchi, Y. *J. Am. Chem. Soc.* **2013**, *135*, 16762−16765.

(24) Jia, Y.; Jiang, Y.; Zhang, J.; Zhang, L.; Chen, Q.; Xie, Z.; Zheng, L. *J. Am. Chem. Soc.* **2014**, *136*, 3748−3751.

(25) Chen, C.; Kang, Y.; Huo, Z.; Zhu, Z.; Huang, W.; Xin, H. L.; Snyder, J. D.; Li, D.; Herron, J. A.; Mavrikakis, M.; Chi, M.; More, K. L.; Li, Y.; Markovic, N. M.; Somorjai, G. A.; Yang, P.; Stamenkovic, V. R. *Science* **2014**, *343*, 1339−1343.

(26) Chen, L. Y.; Guo, H.; Fujita, T.; Hirata, A.; Zhang, W.; Inoue, A.; Chen, M. W. *Adv. Funct. Mater.* **2011**, *21*, 4364−4370.

(27) Ding, Y.; Chen, M. W. *MRS Bull.* **2009**, *34*, 569−576.

(28) Wang, R. Y.; Liu, J.; Liu, P.; Bi, X.; Yan, X.; Wang, W.; Ge, X.; Chen, M. W.; Ding, Y. *Chemical Science* **2014**, *5*, 403−409.

(29) Weissmuller, J.; Newman, R. C.; Jin, H. J.; Hodge, A. M.; Kysar, J. W. *MRS Bull.* **2009**, *34*, 577−586.

(30) Pugh, D. V.; Dursun, A.; Corcoran, S. G. *J. Mater. Res.* **2003**, *18*, 216−221.

(31) Ge, X. B.; Chen, L. Y.; Kang, J. L.; Fujita, T.; Hirata, A.; Zhang, W.; Jiang, J. H.; Chen, M. W. *Adv. Funct. Mater.* **2013**, *23*, 4156−4162.

(32) Wang, R. Y.; Xu, C. X.; Bi, X. X.; Ding, Y. *Energy Environ. Sci.* **2012**, *5*, 5281−5286.

DOI: 10.1021/acscatal.5b00073
ACS Catal. 2015, 5, 3779−3785

(33) Chen, L. Y.; Chen, N.; Hou, Y.; Wang, Z. C.; Lv, S. H.; Fujita, T.; Jiang, J. H.; Hirata, A.; Chen, M. W. *ACS Catal.* **2013**, *3*, 1220−1230.
(34) Erlebacher, J.; Sieradzki, K. *Scr. Mater.* **2003**, *49*, 991−996.
(35) Fujita, T.; Guan, P. F.; McKenna, K.; Lang, X. Y.; Hirata, A.; Zhang, L.; Tokunaga, T.; Arai, S.; Yamamoto, Y.; Tanaka, N.; Ishikawa, Y.; Asao, N.; Yamamoto, Y.; Erlebacher, J.; Chen, M. W. *Nat. Mater.* **2012**, *11*, 775−780.
(36) Toda, T.; Igarashi, H.; Watanabe, M. *J. Electroanal. Chem.* **1999**, *460*, 258−262.
(37) Parida, S.; Kramer, D.; Volkert, C. A.; Rosner, H.; Erlebacher, J.; Weissmuller, J. *Phys. Rev. Lett.* **2006**, *97*, 035504.
(38) Ding, Y.; Kim, Y. J.; Erlebacher, J. *Adv. Mater.* **2004**, *16*, 1897−1900.
(39) Zhang, Z.; Wang, Y.; Qi, Z.; Zhang, W.; Qin, J.; Frenzel, J. *J. Phys. Chem. C* **2009**, *113*, 12629−12636.
(40) Antolini, E.; Salgado, J. R. C.; Gonzalez, E. R. *Appl. Catal., B* **2006**, *63*, 137−149.
(41) Zhang, J.; Ma, J.; Wan, Y.; Jiang, J.; Zhao, X. S. *Mater. Chem. Phys.* **2012**, *132*, 244−247.
(42) Xu, D.; Liu, Z. P.; Yang, H. Z.; Liu, Q. S.; Zhang, J.; Fang, J. Y.; Zou, S. Z.; Sun, K. *Angew. Chem., Int. Ed.* **2009**, *48*, 4217−4221.
(43) Xu, C.; Liu, Y.; Wang, J.; Geng, H.; Qiu, H. *ACS Appl. Mater. Interfaces* **2011**, *3*, 4626−4632.
(44) Stamenkovic, V. R.; Fowler, B.; Mun, B. S.; Wang, G. F.; Ross, P. N.; Lucas, C. A.; Markovic, N. M. *Science* **2007**, *315*, 493−497.
(45) Stephens, I. E. L.; Bondarenko, A. S.; Perez-Alonso, F. J.; Calle-Vallejo, F.; Bech, L.; Johansson, T. P.; Jepsen, A. K.; Frydendal, R.; Knudsen, B. P.; Rossmeisl, J.; Chorkendorff, I. *J. Am. Chem. Soc.* **2011**, *133*, 5485−5491.
(46) Oezaslan, M.; Heggen, M.; Strasser, P. *J. Am. Chem. Soc.* **2012**, *134*, 514−524.
(47) Dutta, I.; Carpenter, M. K.; Balogh, M. P.; Ziegelbauer, J. M.; Moylan, T. E.; Atwan, M. H.; Irish, N. P. *J. Phys. Chem. C* **2010**, *114*, 16309−16320.
(48) Koenigsmann, C.; Sutter, E.; Chiesa, T. A.; Adzic, R. R.; Wong, S. S. *Nano Lett.* **2012**, *12*, 2013−2020.
(49) Koenigsmann, C.; Wong, S. S. *Energy Environ. Sci.* **2011**, *4*, 1161−1176.
(50) Wang, J. X.; Ma, C.; Choi, Y.; Su, D.; Zhu, Y.; Liu, P.; Si, R.; Vukmirovic, M. B.; Zhang, Y.; Adzic, R. R. *J. Am. Chem. Soc.* **2011**, *133*, 13551−13557.
(51) Cui, C.-H.; Li, H.-H.; Liu, X.-J.; Gao, M.-R.; Yu, S.-H. *ACS Catal.* **2012**, *2*, 916−924.

DOI: 10.1021/acscatal.5b00073
ACS Catal. 2015, 5, 3779−3785